

2

WSRC-TR-92-557
Rev 1

Deuterium Absorption and Material Phase Characteristics of SAES St 198 Zr-Fe Alloy (U)

A. Nobile
W. C. Mosley
J. S. Holder
K. N. Brooks

Westinghouse Savannah River Company
Savannah River Site
Aiken, SC 29808



Prepared for the U. S. Department of Energy under Contract No. DE-AC09-89SR18035

MASTER

DISTRIBUTION OF THIS DOCUMENT IS UNLIMITED

Disclaimer

This report was prepared as an account of work sponsored by an agency of the United States Government. Neither the United States Government nor any agency thereof, nor any of their employees, makes any warranty, express or implied, or assumes any legal liability or responsibility for the accuracy, completeness, or usefulness of any information apparatus, produce, or process disclosed, or represents that its use would not infringe privately owned rights. Reference herein to any specific commercial product, process, or service by trade name, trademark, manufacturer, or otherwise does not necessarily constitute or imply its endorsement, recommendation, or favoring by the United States Government or any agency thereof. The views and opinions of authors expressed herein do not necessarily state or reflect those of the United States Government or any agency thereof.



Published in cooperation with WSRC Management Information
Services Section Publications Group.

Technical Editor: Charlie Tope

WSRC-TR-92-557

Rev 1

Publication Date: January 1994

Deuterium Absorption and Material Phase Characteristics of SAES St 198 Zr-Fe Alloy (U)

A. Nobile
W. C. Mosley
J. S. Holder
K. N. Brooks



T. Motyka, Derivative Classifier


J.R. Wermer, Technical Reviewer

Westinghouse Savannah River Company
Savannah River Site
Aiken, SC 29808



Prepared for the U. S. Department of Energy under Contract No. DE-AC09-89SR18035

DISTRIBUTION OF THIS DOCUMENT IS UNLIMITED 

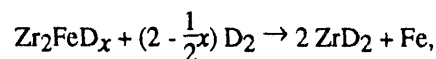
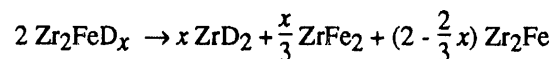
This page intentionally left blank.

Abstract

This document reports on deuterium absorption and material phase characteristics of SAES St 198 Zr-Fe Alloy. Scanning electron microscope images of polished surfaces, electron probe microanalysis, and x-ray powder diffractometry indicated the presence of a primary Zr_2Fe phase with secondary phases of $ZrFe_2$, Zr_3FeSn , α -Zr, and Zr_6Fe_3O . A statistically designed experiment to determine the effects of temperature, time, and vacuum quality on activation of St 198 revealed that, when activated at low temperature (350°C), deuterium absorption rate was slower when the vacuum quality was poor (2.5 Pa vs. 3×10^{-4} Pa). However, at higher activation temperature (500°C), deuterium absorption rate was fast and was independent of vacuum quality. Deuterium pressure-composition-temperature (P-C-T) data are reported for St 198 in the temperature range 200°C to 500°C. The P-C-T data over the full range of deuterium loading and at temperatures of 350°C and below is described by the following expression in terms of the equilibrium deuterium absorption pressure, P_{D_2} , and the getter loading, q :

$$K_o e^{-(\Delta H_a/RT)} = \frac{(q^*-q)^2}{P_{D_2} q^2},$$

where ΔH_a and K_o have values of 101.8 kJ·mole⁻¹ and 3.24×10^{-8} Pa⁻¹, respectively, and q^* is 15.998 kPa·L⁻¹·g⁻¹. At higher temperatures, one or more secondary reactions in the solid phase occur that slowly consume D_2 from the gas phase. X-ray diffraction and other data suggest these reactions to be:



where $0 < x < 3$. Reaction between gas-phase deuterium and Zr_2Fe formed in the first reaction accounts for the observed consumption of deuterium from the gas phase by this reaction.

This page intentionally left blank.

Contents

| | |
|--|----|
| Abstract | i |
| Introduction | 1 |
| Experimental | 2 |
| Elemental Analysis | 2 |
| Pellet Physical Properties | 2 |
| Material Phase Characteristics | 2 |
| Activation Study | 3 |
| Pressure-Composition-Temperature Measurements | 3 |
| Results | 3 |
| Elemental Analysis | 3 |
| Pellet Physical Properties | 5 |
| Material Phase Characteristics | 8 |
| Activation Study | 10 |
| Pressure-Composition-Time Measurements | 14 |
| X-Ray Diffraction Analysis of Deuterium-Loaded Samples | 20 |
| Discussion | 22 |
| Conclusion | 25 |
| Acknowledgments | 25 |
| References | 25 |

List of Figures

| | |
|---|----|
| 1. Schematic Arrangement of the Apparatus Used for Activation and P-C-T studies on St 198 Samples (a), Sample Cell (b) | 4 |
| 2. Scanning Electron Microscopy Image of an As-Received SAES St 198 Pellet Surface | 6 |
| 3. Incremental Intrusion Volume vs. Pore Diameter for As-Received SAES St 198 Pellets | 7 |
| 4. Scanning Electron Microscopy BSE Image and Elemental Maps of the Polished Surface of an As-Received St 198 Pellet | 9 |
| 5. X-Ray Powder Diffraction Patterns of SAES St 198 Powder from Pulverized As-Received Pellets | 11 |

| | | |
|-----|--|----|
| 6. | Deuterium Pressure vs. Time Data for Three Sets of Conditions in the 2 ³ Factorial Test | 12 |
| 7. | $\text{Log}(P/P_0)$ vs. Time Plots Used to Determine Initial Deuterium Absorption Rates in the 2 ³ Factorial Test | 13 |
| 8. | Deuterium Absorption Isotherms for SAES St 198 | 15 |
| 9. | Deuterium Absorption Isotherms at 500°C for Equilibration Times of 20 minutes and 1 Hour for SAES St 198 | 17 |
| 10. | Absorption Pressure vs. $q^2/(q^*-q)^2$ for SAES St 198 at Temperatures of 200°C, 300°C, and 350°C | 18 |
| 11. | van't Hoff Plot of the Equilibrium Constants | 19 |
| 12. | X-Ray Powder Diffraction Patterns of SAES St 198 Samples After Conducting Absorption Isotherms at 200°C and 500°C | 21 |

List of Tables

| | | |
|----|--|----|
| 1. | Elemental Analysis of As-received SAES St 198 by Inductively Coupled Plasma Mass Spectroscopy and X-Ray Fluorescence | 5 |
| 2. | Summary of As-Received SAES St 198 Pellet Physical Characterization Parameters | 8 |
| 3. | Test Matrix and Results for 2 ³ Factorial Getter Activation Test | 14 |
| 4. | Main Effects Values Determined from 2 ³ Factorial Test | 14 |
| 5. | Relative Intensities of the Strongest XRD Peaks for As-Received and Deuterium-Exposed SAES St 198 | 20 |

Introduction

A metal getter having a reported composition of 76.5%Zr · 23.5%Fe, which is produced and sold by SAES Getters under the trade name St 198, has the unique property of being reactive with hydrogen isotopes, oxygen, water, and other gases, while remaining relatively unreactive toward nitrogen. Further, the material is available as pressed pellets that can be used in packed bed reactors with minimal gas pressure drop. These properties allow this getter to be a candidate for tritium removal from nitrogen glovebox atmospheres and inert gas process streams with low tritium concentrations. The advantage of removing tritium from glovebox atmospheres with metal getters is that highly radiotoxic tritiated water is not formed, as with conventional glovebox tritium removal systems that catalytically oxidize tritium to water and trap tritiated water on molecular sieves.

Kherani et al.¹ studied tritium removal from flowing nitrogen using a SAES St 198/707 purifier cartridge. They were able to remove tritium in nitrogen with initial concentrations less than 1 mCi·m⁻³ to levels undetectable by their ion chamber. However, for initial concentrations higher than 1 mCi·m⁻³, tritium broke through. The amount of breakthrough increased with flow and initial tritium concentration. Ontario Hydro Research Division² designed and built a glovebox tritium cleanup system that uses St 198. In fact, in a collaborative effort between SAES Getters and Ontario Hydro Research, a tritium cleanup system using St 198 was designed for commercial sale. The Ontario Hydro Research glovebox unit successfully removed tritium from the glovebox atmosphere during tests. However, tritium breakthrough behavior at higher tritium concentrations happened, similar to that observed by Kherani et al.¹

The above work demonstrated the usefulness of St 198 for tritium cleanup systems. The improvements to the getter bed design will likely eliminate tritium breakthrough at higher concentrations and flow. At the Savannah River Site (SRS), a program is underway to develop technology that uses metal getters to remove tritium from glovebox and process atmospheres. Our experience with metal hydride tritium handling processes demonstrated that a thorough understanding of hydrogen isotope absorption properties and material phase characteristics of metal hydride forming materials is essential for many reasons. This document reports results from the deuterium pressure-composition-temperature (P-C-T) behavior and the material phase characteristics of St 198. We also investigated the getter activation and undesirable secondary reactions, which occur in the Zr₂Fe lattice at high temperature while loaded with deuterium. Additionally, we report a number of physical parameters such as densities and pore structure data that are useful for metal getter reactor design calculations.

Some data on the hydrogen absorption behavior of Zr₂Fe exists in the literature. Manini et al.³ and Boffito et al.⁴ provide hydrogen absorption isotherms for St 198 at temperatures between 200°C and 700°C. Both of these publications provide correlations that relate the hydrogen absorption pressure to temperature and getter hydrogen content. While the material has a total hydrogen capacity approaching 16 kPa·L·g⁻¹, the correlation of Manini et al.³ applies to hydrogen loadings of less than 1.5 kPa·L·g⁻¹. The correlation reported by Boffito et al.⁴ applies to hydrogen loadings less than 0.66 kPa·L·g⁻¹. Manini et al.³ also report, that at temperatures higher than

500°C, hydrogen never reached equilibrium with the material, apparently because of a slow reaction of Zr_2FeH_x to ZrH_2 and Zr_2Fe . These works further show that at low hydrogen loading Zr_2FeH_x is only partially converted to ZrH_2 and Zr_2Fe . At high loadings ZrH_2 and Zr_2Fe are completely converted. The samples of Manini et al. were held at 500°C for 2 hours. Van Essen and Buchow⁵, who investigated hydrogen absorption in several Zr- and Hf-based intermetallic compounds, state that hydrogen uptake in Zr_2Fe does not form a stable hydride, but decomposes to Zr_2Fe and ZrH_2 when activated for 4 hours at 50°C and under 4.05 MPa of hydrogen pressure. Aubertin and coworkers⁶ confirmed decomposition of hydrogen-loaded Zr_2Fe to Zr_2Fe and ZrH_2 when Zr_2Fe was exposed at 850°C to 100 kPa of hydrogen for 15 hours.

Experimental

Elemental Analysis

We purchased the St 198 getter as 4 mm long × 6 mm diameter pressed pellets from SAES Getters USA, Colorado Springs, Colorado. Using solutions obtained by acid dissolution of the getter, we analyzed by inductively coupled plasma-mass spectroscopy (ICP-MS) the getter elemental composition. We dissolved the getter by adding 0.1 g of sample to 8 mL of aqua regia, followed by overnight heating at 95°C. A remaining residue was then dissolved by adding 2 mL of HF. This solution was then diluted for analysis by ICP-MS. Getter material was also analyzed by x-ray fluorescence (XRF) without standards, but this method is qualitative, and is not expected to be as accurate as ICP-MS.

Pellet Physical Properties

The pore structure of St 198 pellets was characterized with a Micromeritics Auto-Pore II Model 9220 mercury intrusion porosimeter. A number of parameters such as void fractions, densities of pellets, and a packed bed of the as-received pellets were measured.

Material Phase Characteristics

Scanning electron microscopy (SEM) provided images of polished surfaces on St 198 pellets to visually examine the phases present in the material. Energy dispersive x-ray (EDX) yielded qualitative elemental analyses of selected areas on the particle surface. Electron probe microanalysis (EPMA) provided quantitative analyses of selected areas. X-ray intensities were compared with zirconium, iron, and tin standards using corrections for atomic number, absorption, and fluorescence (ZAF corrections). We performed x-ray diffractometry (XRD) on powder from crushing St 198 pellets. Copper K-alpha radiation was used to scan the two theta range from 5°C to 135°C. Phases were identified by matching crystallographic diffraction peak interplanar spacings (d -values) and relative intensities with reference XRD data.⁷

Activation Study

We activated the St 198 getter by holding samples under vacuum above 350°C for several hours. During activation, oxygen from oxides on particle surfaces supposedly diffuses into the bulk, producing highly reactive surfaces. To determine the optimum activation conditions and the effects of temperature, time, and vacuum quality on material activation, we performed a 2³ factorial experiment. Samples were activated at temperatures of 350°C and 500°C, for periods of 4 and 16 hours, and under evacuation by a Welch Duo-Seal two-stage rotary vane pump (2.5 Pa) or an Alcatel Drytel 30 fluidless vacuum pump (3×10^{-4} Pa). A cold trap was not used with either pump. The extent of activation was determined by measuring the initial deuterium absorption rate at 350°C. High initial deuterium absorption rate indicates a well activated sample. We measured the absorption rate on the gas manifold (Figure 1a). Samples (~ 1 g) were held in the sample cell (Figure 1b), which was wrapped with electrical heating tape. A temperature controller kept the sample temperature constant within 1°C. After activating the sample, a data acquisition computer recorded pressure vs. time data after a valve between the sample and a 300 mL calibrated volume that contained 4000 Pa (30 torr) of deuterium opened. An MKS Baratron 390H 0-133 kPa capacitance manometer measured the pressure.

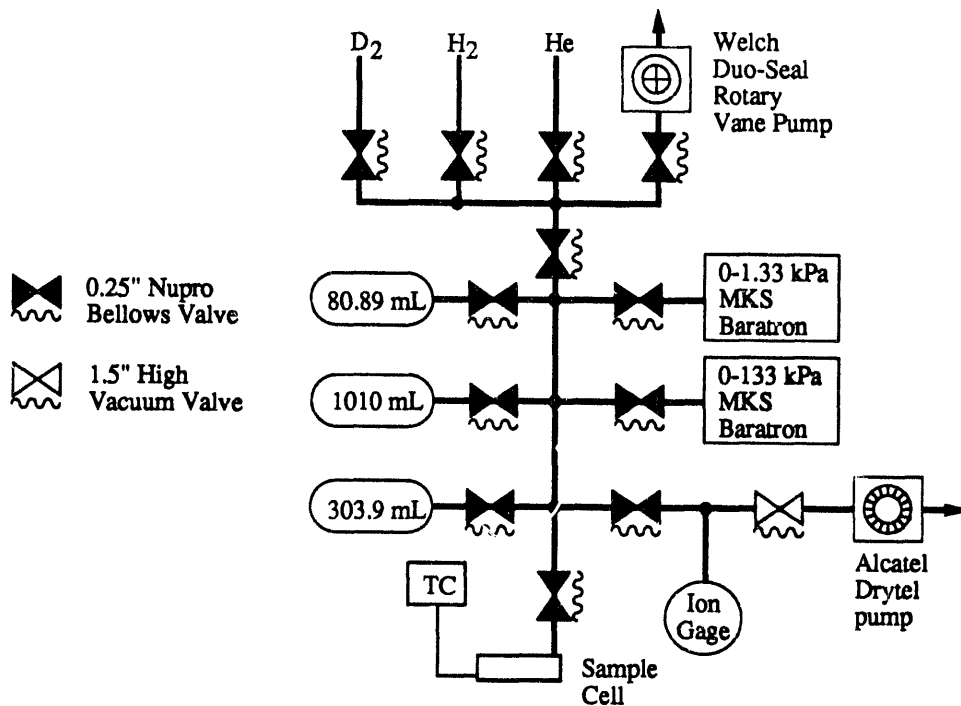
Pressure-Composition-Temperature Measurements

We investigated deuterium P-C-T behavior for St 198 samples using the same gas manifold, sample cell, and sample size described above. We measured absorption isotherms at temperatures from 200°C to 500°C. Before each isotherm measurement, we loaded a fresh sample into the sample cell and activated the cell by evacuating it with an Alcatel Drytel 30 vacuum pump to $<3 \times 10^{-4}$ Pa at 350°C for 4 hours. A data acquisition computer was used to automate static absorption isotherm measurements. After admitting an aliquot of gas to the sample, the sample equilibrated for 20 minutes. A 0-1.33 kPa MKS Baratron 390H capacitance manometer measured the pressure in equilibrium with the samples.

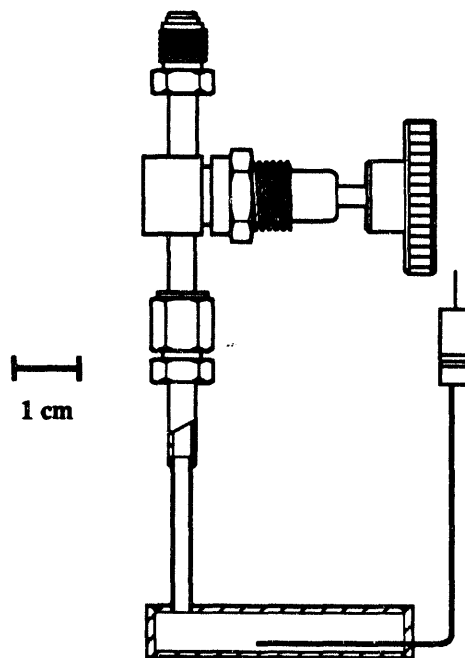
Results

Elemental Analysis

Table 1 shows the results from ICP-MS and XRF elemental analyses of St 198. Boffito et al.⁴ reported St 198 to have the composition 76.5 wt. % Zr, 23.5 wt. % Fe. Our iron analysis agrees closely with that of Boffito et al., but we detected slightly less zirconium and some tin (1.2%). Zn, Cu, Ti, La, and Cr are most likely impurities, and probably do not influence the getter behavior significantly. As will be shown below, tin plays a role in the phase behavior of the material. XRF analysis is only qualitative and does not agree with ICP-MS. However, XRF shows the presence of copper, which was not detected by ICP-MS.



(a)



(b)

Figure 1. Schematic Arrangement of the Apparatus Used for Activation and P-C-T Studies on St 198 Samples (a), Sample Cell (b)

Table 1. Elemental Analysis of As-received SAES St 198 by Inductively Coupled Plasma Mass Spectroscopy and X-Ray Fluorescence

| Element | Weight Percent | |
|---------|----------------|------|
| | ICP-MS | XRF |
| Zr | 73.60 | 81.8 |
| Fe | 23.30 | 6.9 |
| Sn | 1.20 | 1.0 |
| Zn | 0.50 | - |
| Cu | - | 0.3 |
| Ti | 0.10 | - |
| La | 0.07 | - |
| Cr | 0.06 | - |

Pellet Physical Properties

St 198 pellets are formed by compacting irregular alloy granules with maximum dimensions of about 150 μm (Figure 2). Figure 3 shows pore size distribution data for St 198 pellets expressed as incremental intrusion volume vs. diameter. The majority of the pores are in the 2 to 5 μm diameter range, with most remaining pores in the 0.2 to 2 μm range. The material has few pores with diameters less than 0.1 μm . Each 6 mm diameter \times 4 mm long St 198 pellet weighed 0.6 g, corresponding to a pellet density of 5.3 $\text{g}\cdot\text{cm}^{-3}$, which closely agrees with 5.17 measured by porosimetry. The theoretical density of 6.8697 $\text{g}\cdot\text{cm}^{-3}$ measured by porosimetry agrees with 6.938 $\text{g}\cdot\text{cm}^{-3}$ for Zr_2Fe obtained from x-ray powder diffraction files.⁷

The void fraction of 0.25 calculated from the pellet and theoretical densities in Table 2 are slightly lower than the value of 0.31 that we determined from gas expansion measurements. The higher value obtained by gas expansion suggests the presence of small pores not accessible by the mercury intrusion method. However, the close agreement between theoretical densities obtained from the powder diffraction files and porosimetry is inconsistent with inaccessible porosity in the sample. It is more likely that the deviation is attributable to the larger error associated with the gas expansion technique. Thus, the value from the porosimetry measurements is probably more reliable.

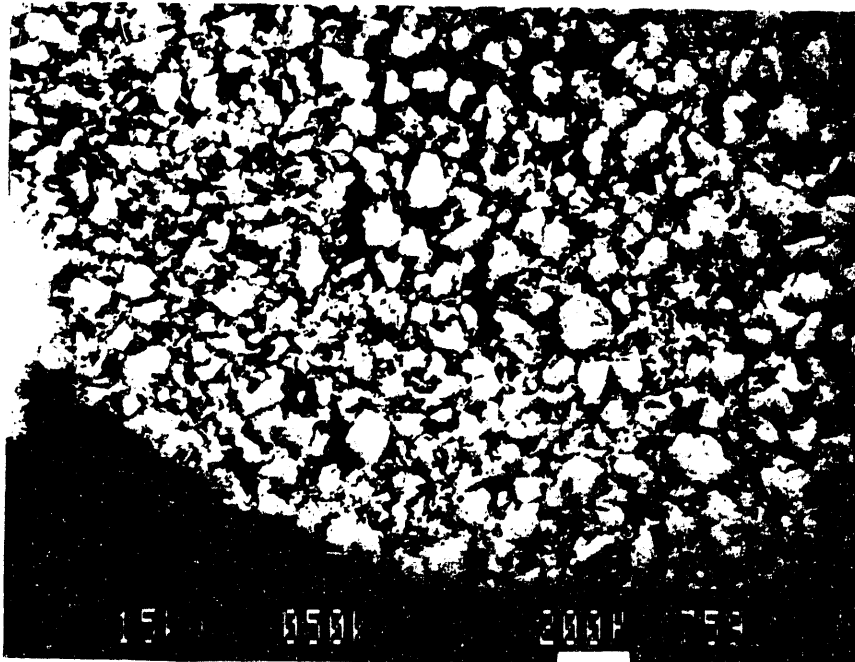


Figure 2. Scanning Electron Microscopy Image of an As-Received SAES St 198 Pellet Surface

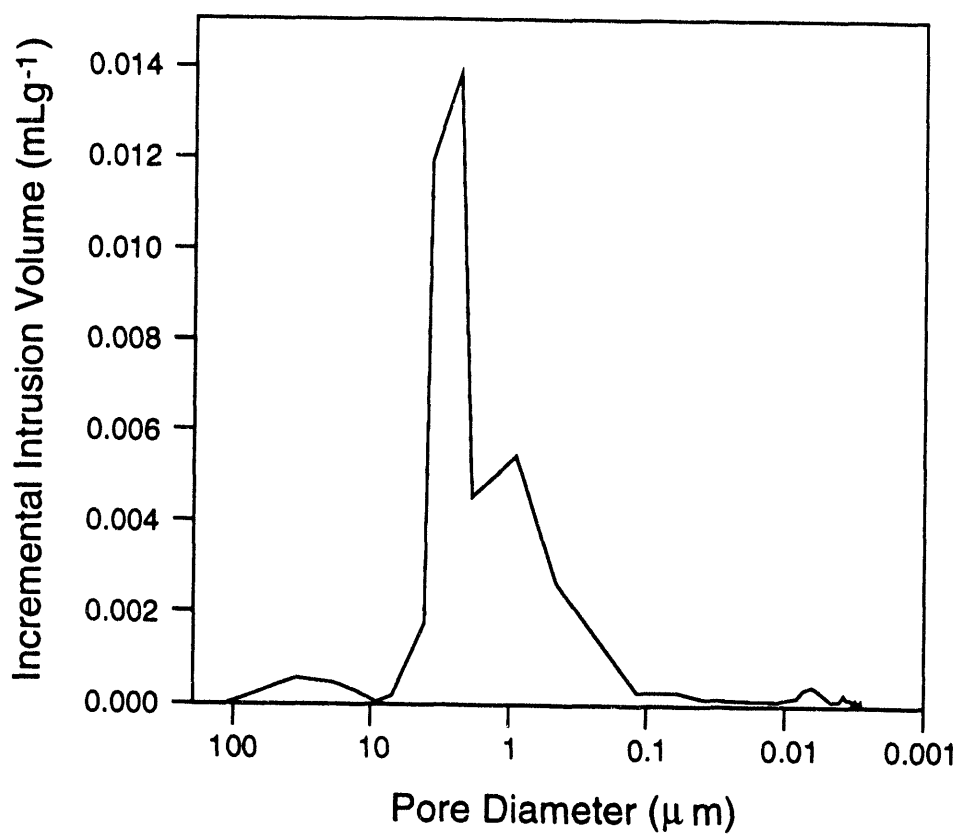


Figure 3. Incremental Intrusion Volume vs. Pore Diameter for As-Received SAES St 198 Pellets

| Property | Value |
|---|---------------------------------------|
| Total intrusion volume | 0.0479 mL·g ⁻¹ |
| Total pore area | 2.523 m ² ·g ⁻¹ |
| Median pore diam (vol) | 2.8443 μm |
| Median pore diam (area) | 0.0042 μm |
| Average pore diam (4V/A) | 0.0759 μm |
| Pellet density | 5.1689 g·mL ⁻¹ |
| Theoretical density | 6.8697 g·mL ⁻¹ |
| Pellet void fraction | 0.25 |
| Packed bed void fraction (4 mm × 6 mm pellets) | 0.43 |

The tap density of a packed bed of 4 mm long × 6 mm diameter pellets was measured to be 2.93 g·mL⁻¹. From this, a void fraction of 0.43 for the bed is calculated, and represents the void fraction associated with volume between individual pellets in the bed.

Material Phase Characteristics

Figure 4 shows an SEM backscattered electron (BSE) image of the polished surface of an St 198 pellet. Five phases were detected. The intensity (brightness) of a phase in a BSE image is a function of the phase composition with brightness increasing with average atomic number. The primary phases in St 198 has medium intensity. The composition of the primary phase was determined from EPMA lines profiles to be $Zr_{0.660 \pm 0.018}Fe_{0.337 \pm 0.019}Sn_{0.003 \pm 0.001}$ that corresponds to Zr_2Fe . The composition of the dark, blocky secondary phase is $Zr_{0.350 \pm 0.010}Fe_{0.650 \pm 0.010}$ that corresponds to $ZrFe_2$. A large portion of St 198 is eutectic consisting of primary Zr_2Fe with micrometer-size inclusions of bright secondary phases. SEM/EDX showed that one bright secondary phase was nearly pure zirconium and another contained zirconium, iron, and tin. EPMA was not able to resolve the two bright secondary phases in the inclusions in the eutectic. Analyses in eutectic yielded an average composition of 73.3 ± 1.6 atomic percent (a/o) zirconium, 25.5 a/o iron and 1.2 ± 0.6 a/o tin. However, three points in a large isolated area of a bright secondary phase yielded $Zr_{0.715 \pm 0.01}Fe_{0.151 \pm 0.019}Sn_{0.130 \pm 0.026}$, which corresponds to Zr_5FeSn . Small inclusions within the eutectic with the same intensity are thought to be Zr_5FeSn . Two EMPA analysis points corresponded to nearly pure zirconium with 79 a/o Zr, 17.7 a/o Fe and 3.3 a/o Sn and 82.8 a/o Zr, 13.0 a/o Fe and 4.3 a/o Sn. Scattered dark areas detected within the primary phase by BSE/SEM are thought to correspond to an oxide phase. Figure 5 shows an XRD pattern for as-received St 198 and indicated the presence of four phases: Zr_2Fe , $ZrFe_2$, a-Zr and Zr_6FeO .⁷ No lines of an XRD pattern for Zr_5FeSn were detected.

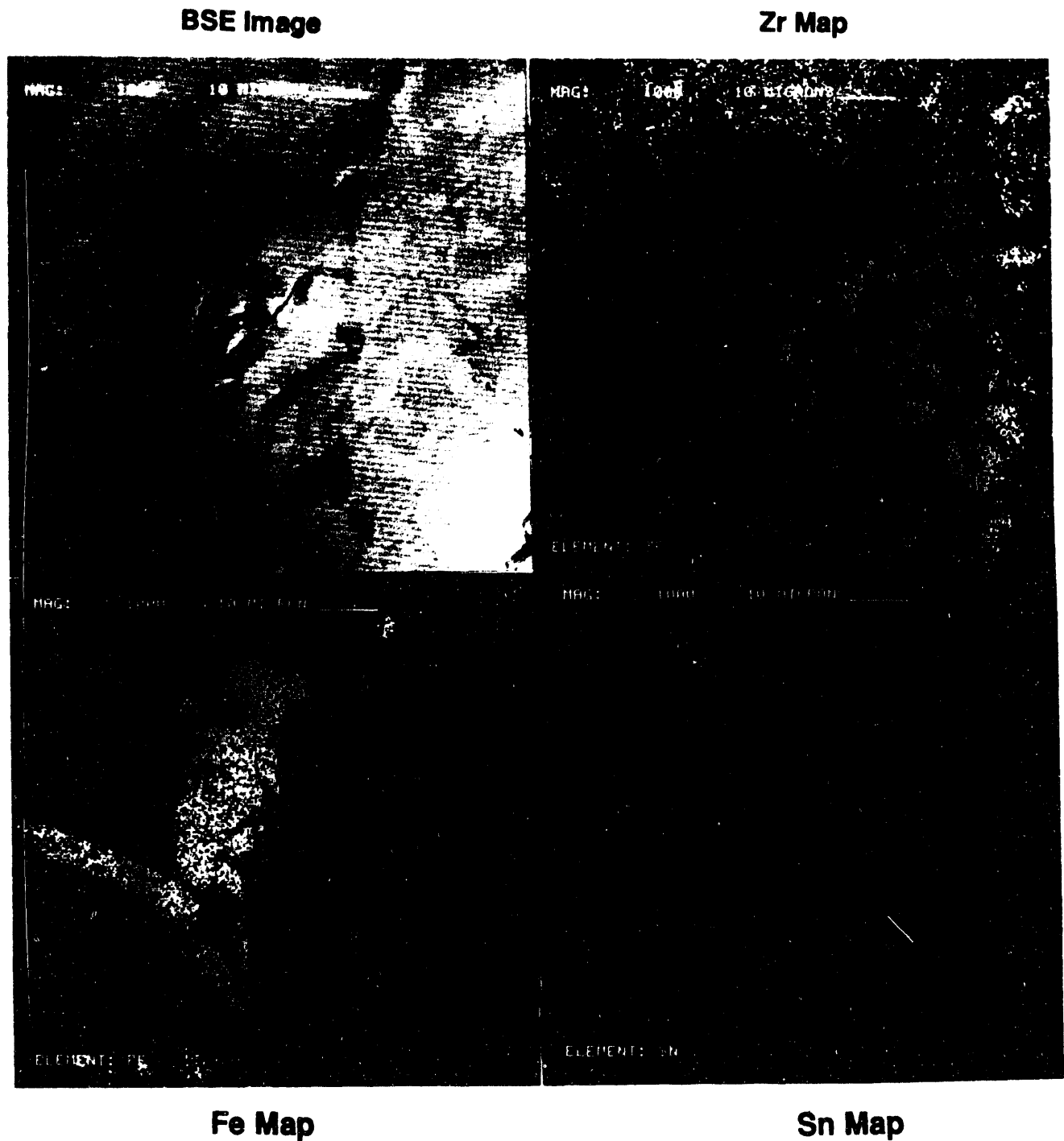


Figure 4. Scanning Electron Microscopy BSE Image and Elemental Maps of the Polished Surface of an As-Received St 198 Pellet

Activation Study

We determined initial absorption rates for activated samples from deuterium pressure vs. time data that was modeled with the rate equation:

$$(1) \quad \frac{RT}{w} \frac{dn_{D_2}}{dt} = \frac{V}{w} \frac{dP}{dt} = k_a P,$$

which when integrated gives the expression

$$(2) \quad 2.303 \log\left(\frac{P}{P_0}\right) = \frac{V}{w} k_a t,$$

where w is the weight of the sample, n_{D_2} is the number of moles of deuterium, V is the system volume, P and P_0 are the pressure and starting pressure, respectively, and k_a is an absorption rate constant. Thus, a plot of $\log(P/P_0)$ vs. time has slope $(V/2.303w)k_a$ and zero intercept. Figure 6 shows pressure vs. time curves for three different sets of activation conditions and Figure 7 shows $\log(P/P_0)$ vs. time for these data for the first 2 seconds. Once k_a is determined by linear regression of the first 2 seconds of the absorption data, the initial rate ($\text{kPa}\cdot\text{L}\cdot\text{s}^{-1}\cdot\text{g}^{-1}$) is calculated from

$$(3) \quad \frac{RT}{w} \left(\frac{dn_{D_2}}{dt} \right)_{t=0} = k_a P_0.$$

Table 3 shows the various activation conditions studied and the resulting initial deuterium absorption rates from the 2^3 factorial experiment. With the exception of samples activated at low temperature and under higher vacuum pressure (oil-sealed rotary vane pump), all initial absorption rates had values between 0.414 and 0.773 $\text{kPa}\cdot\text{L}\cdot\text{s}^{-1}\cdot\text{g}^{-1}$. Samples activated under higher pressure and at low temperature yielded significantly lower initial absorption rates.

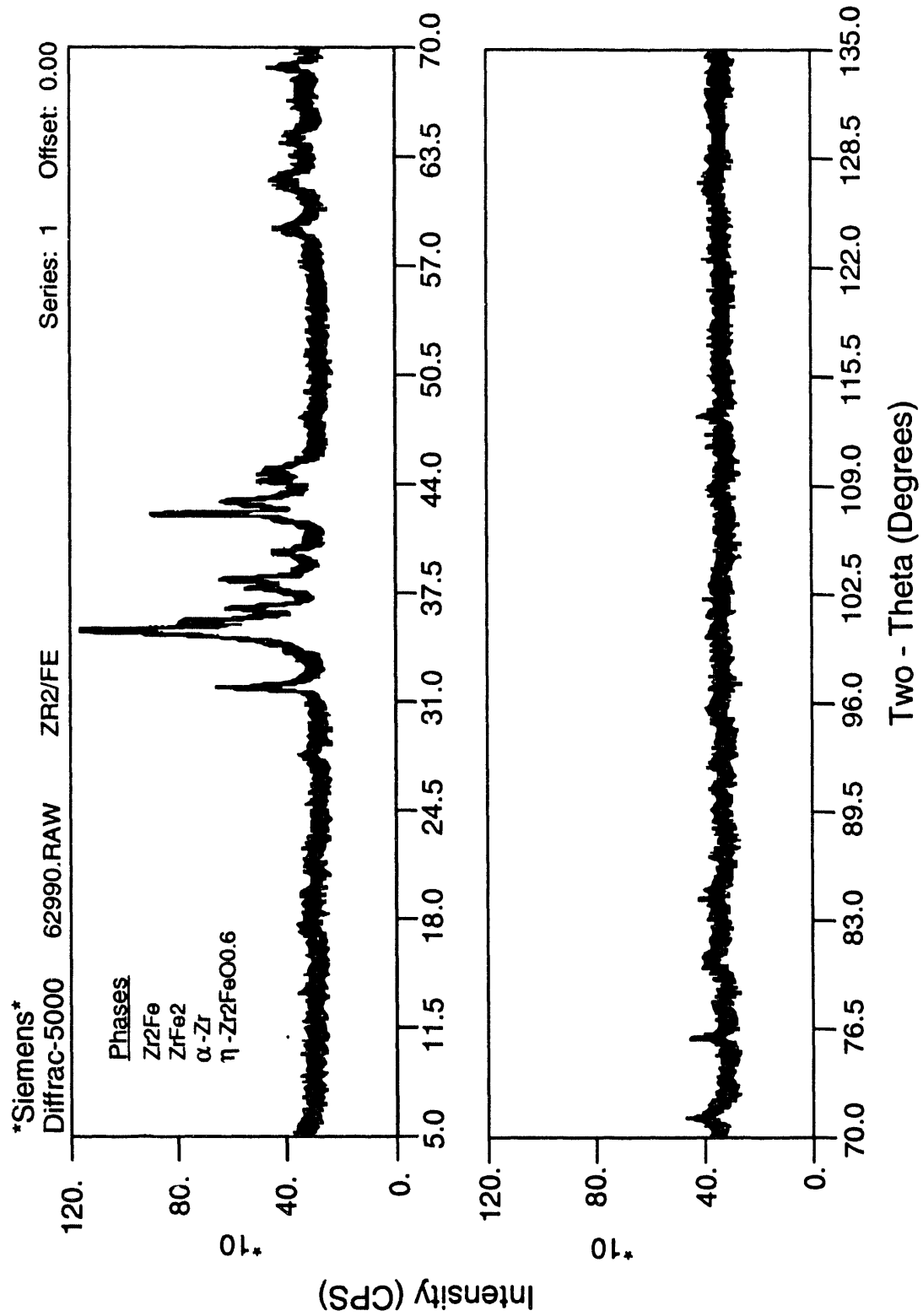


Figure 5. X-Ray Powder Diffraction Patterns of SAES St 198 Powder from Pulverized As-Received Pellets

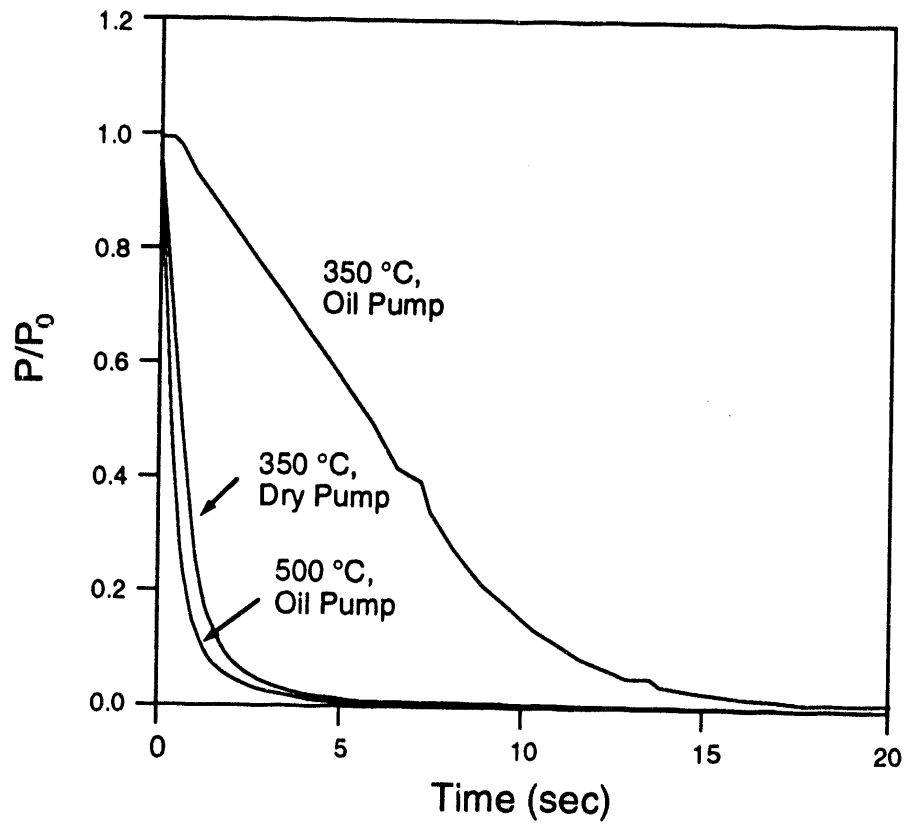


Figure 6. Deuterium Pressure vs. Time Data for Three Sets of Conditions in the 2^3 Factorial Test

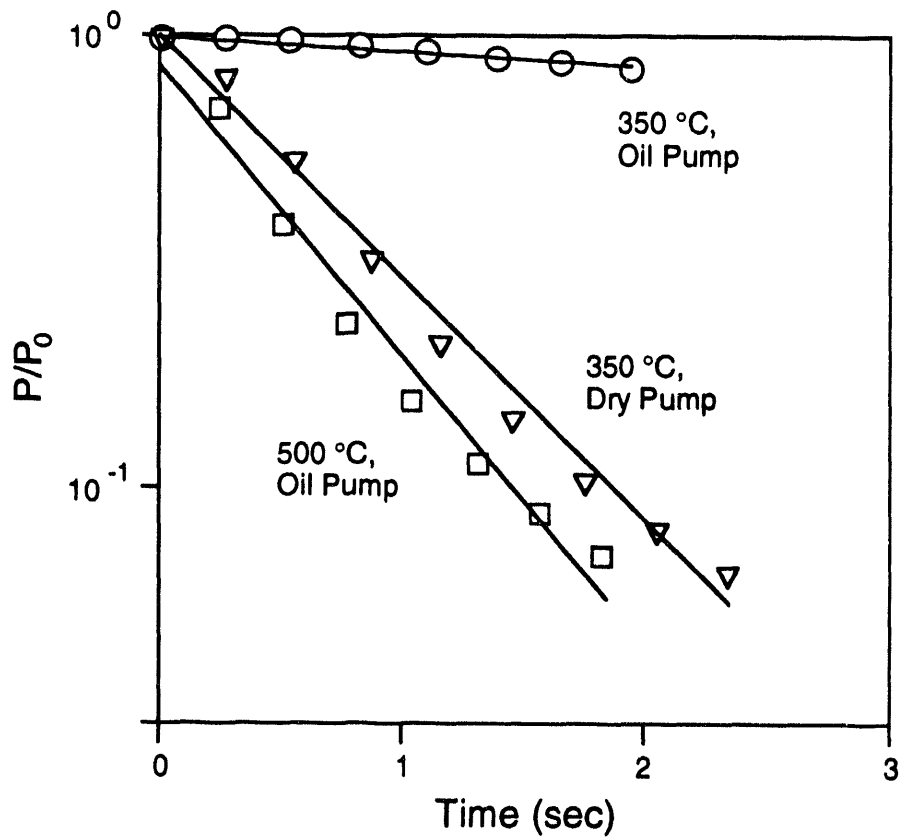


Figure 7. $\text{Log}(P/P_0)$ vs. Time Plots Used to Determine Initial Deuterium Absorption Rates in the 2^3 Factorial Test

Table 3. Test Matrix and Results for 2³ Factorial Getter Activation Test

| Run | Temperature (°C) | Activation (hour) | VAC Press (Pa) | Rate (kPa·L·s ⁻¹ ·g ⁻¹) |
|-----|------------------|-------------------|----------------------|--|
| 1 | 500 | 4 | 2.5 | 0.7468 |
| 2 | 500 | 4 | 3 × 10 ⁻⁴ | 0.5377 |
| 3 | 500 | 16 | 2.5 | 0.4140 |
| 4 | 500 | 16 | 3 × 10 ⁻⁴ | 0.7730 |
| 5 | 350 | 4 | 2.5 | 0.0430 |
| 6 | 350 | 4 | 3 × 10 ⁻⁴ | 0.6028 |
| 7 | 350 | 16 | 2.5 | 0.0017 |
| 8 | 350 | 16 | 3 × 10 ⁻⁴ | 0.6829 |

Table 4 shows the main effects calculated from the statistical test. The main effect is a relative number that indicates the relative effect of each variable on the response parameter (initial absorption rate). The larger the main effect, the greater the effect of the variable on the response parameter. Temperature and vacuum conditions have the largest effect on the initial absorption rate, whereas time does not appear to affect the activation process significantly.

Table 4. Main Effect Values Determined from 2³ Factorial Test

| Variable | Main Effect |
|------------------|-------------|
| Temperature | 0.285 |
| Time | -0.015 |
| Vacuum Condition | -0.348 |

Pressure-Composition-Time Measurements

Figure 8 shows deuterium absorption isotherms for Zr₂Fe at temperatures between 200°C and 500°C. At approximately 6 kPa·L·g⁻¹, the slope of the 400°C isotherm decreases and the isotherm eventually contacts the 350°C isotherm at approximately 10 kPa·L·g⁻¹. Similarly, the isotherm at 500°C undergoes a slope change at about 5 kPa·L·g⁻¹ and nearly contacts the isotherms at 350°C and 400°C. During measurement of the 500°C isotherm,

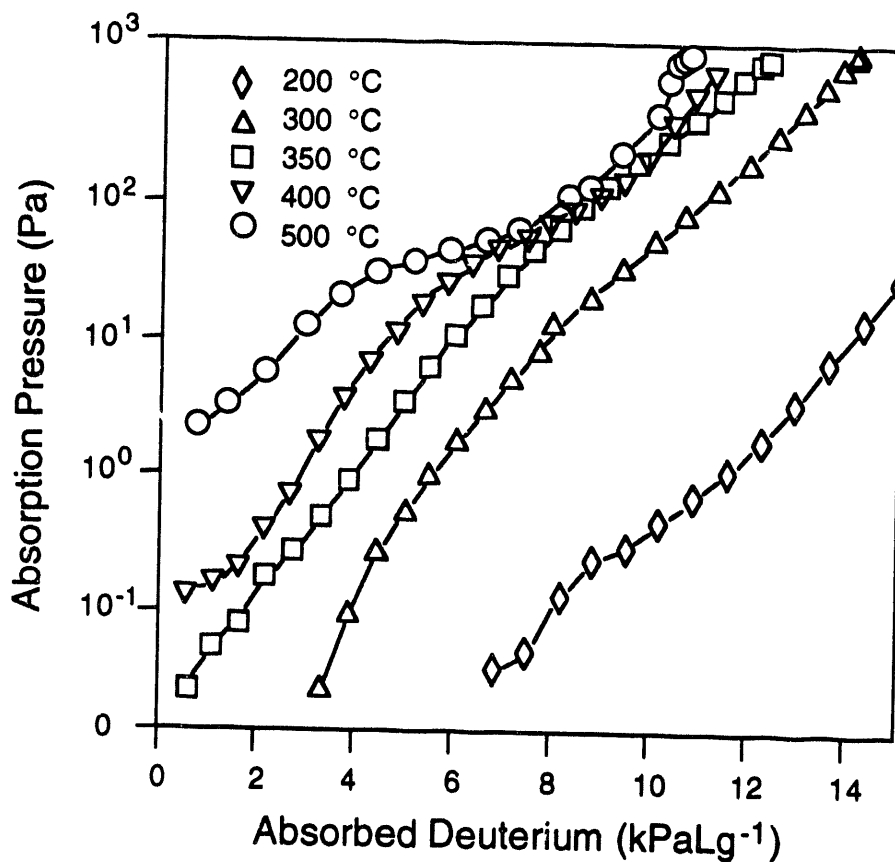


Figure 8. Deuterium Absorption Isotherms for SAES St 198

we observed that there was initially a rapid equilibration of D_2 with the getter, which was complete within a few seconds. However, a slow decrease in system pressure followed the equilibration. At the lower temperature ($<350^\circ\text{C}$) equilibration occurred within a few seconds, but the final pressure was stable. This observation indicated that initial deuterium equilibration with the sample was rapid, but that a slow solid state reaction occurred and consumed gas-phase deuterium. After running the isotherm again (Figure 9) with a longer equilibration time (1 hour), it was apparent that at loadings higher than approximately $2 \text{ kPa}\cdot\text{L}\cdot\text{g}^{-1}$, a reaction that consumed additional deuterium from the gas phase was occurring. Absorption isotherms at 350°C run at 20 minutes and 1 hour were the same. This rate of the secondary reaction on the time scale indicates the isotherm measurement is insignificant at 350°C .

Further observation of the absorption isotherms in Figure 8 indicates that there appears to be no α -phase-hydride phase transition. The fact that the isotherms are continuous indicates that deuterium absorption occurs by solution of deuterium atoms into the bulk lattice with no abrupt lattice phase transition. Given this, it is possible to describe the equilibrium thermodynamics with a simple chemical equilibrium expression. The following can be written for the reaction of deuterium gas with lattice deuterium sites:



where S is a vacant absorption site. The equilibrium expression for this reaction is,

$$(5) \quad K_{eq} = \frac{[DS]^2}{P_{D_2} [S]^2},$$

where K_{eq} is the equilibrium constant, P_{D_2} is the deuterium partial pressure, and $[S]$ and $[DS]$ are the concentrations of vacant, and deuterium-occupied sites in the metal lattice, respectively. This expression can also be written in terms of the getter loading, q , and the value of q at full loading, q^* ,

$$(6) \quad P_{D_2} = \frac{q^2}{K_{eq}(q^* - q)^2}$$

A value of $15.998 \text{ kPa}\cdot\text{L}\cdot\text{g}^{-1}$ was used for q^* . A plot of P_{D_2} vs. $q^2/(q^* - q)^2$ would be a straight line with slope $1/K_{eq}$. Figure 10 shows this plot for the P-C-T data of Figure 8 at temperatures of 350°C and below. At the higher temperatures, because of the slow reaction occurring in the lattice, the data deviated significantly from the model, so these data were excluded from Figure 10. A van't Hoff plot of the equilibrium constants determined from the slope of the lines in Figure 10 is shown in Figure 11. The value of the equilibrium constant at 400°C is plotted on Figure 11. This point deviates significantly from the data at lower temperatures. From the slope of this plot, an absorption enthalpy, ΔH_a of $101.8 \text{ kJ}\cdot\text{mole}^{-1}$, is calculated. Thus, the deuterium P-C-T data for the full range of loadings and at temperatures of 350°C and below are described by,

$$(7) \quad K_0 e^{-(\Delta H_a/RT)} = \frac{(q^* - q)^2}{P_{D_2} q^2},$$

where K_0 was determined from the intercept of Figure 11 to be $3.24 \times 10^{-8} \text{ Pa}^{-1}$.

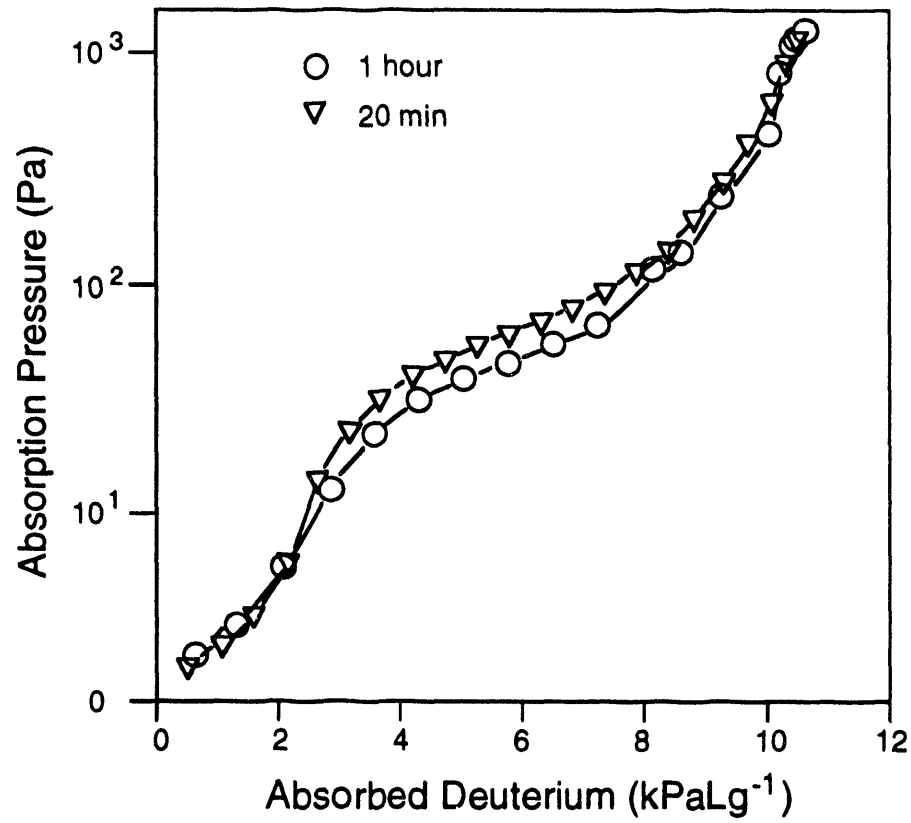


Figure 9. Deuterium Absorption Isotherms at 500°C for Equilibration Times of 20 Minutes and 1 Hour for SAES St 198

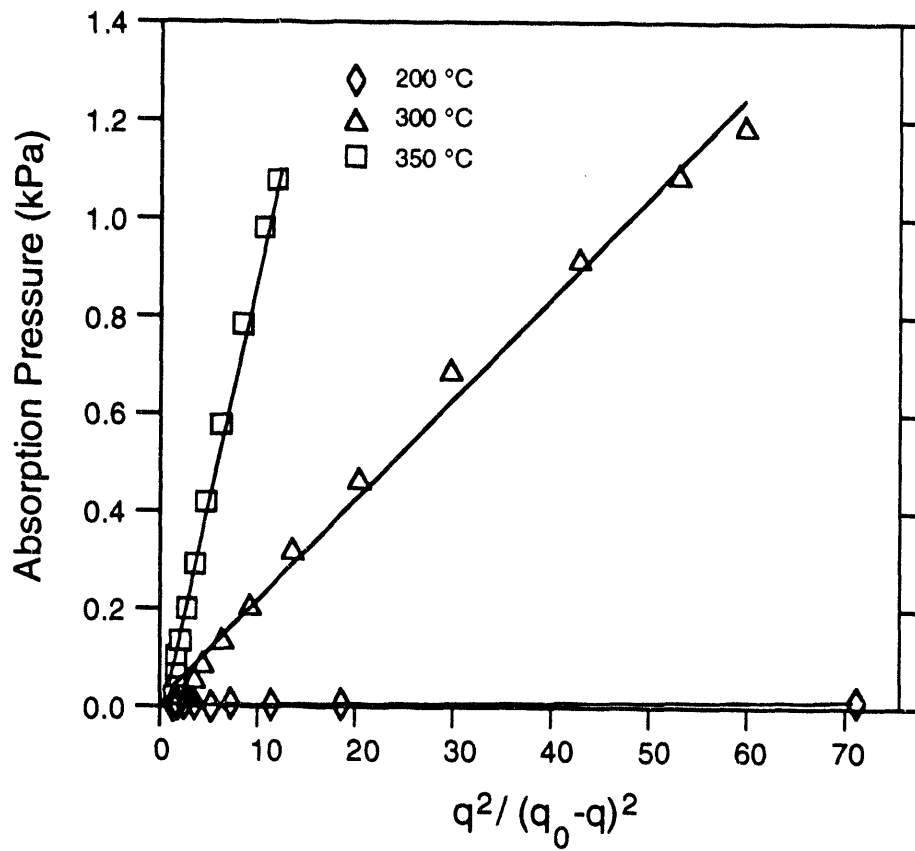


Figure 10. Absorption Pressure vs. $q^2 / (q_0 - q)^2$ for SAES St 198 at Temperatures of 200°C, 300°C, and 350°C

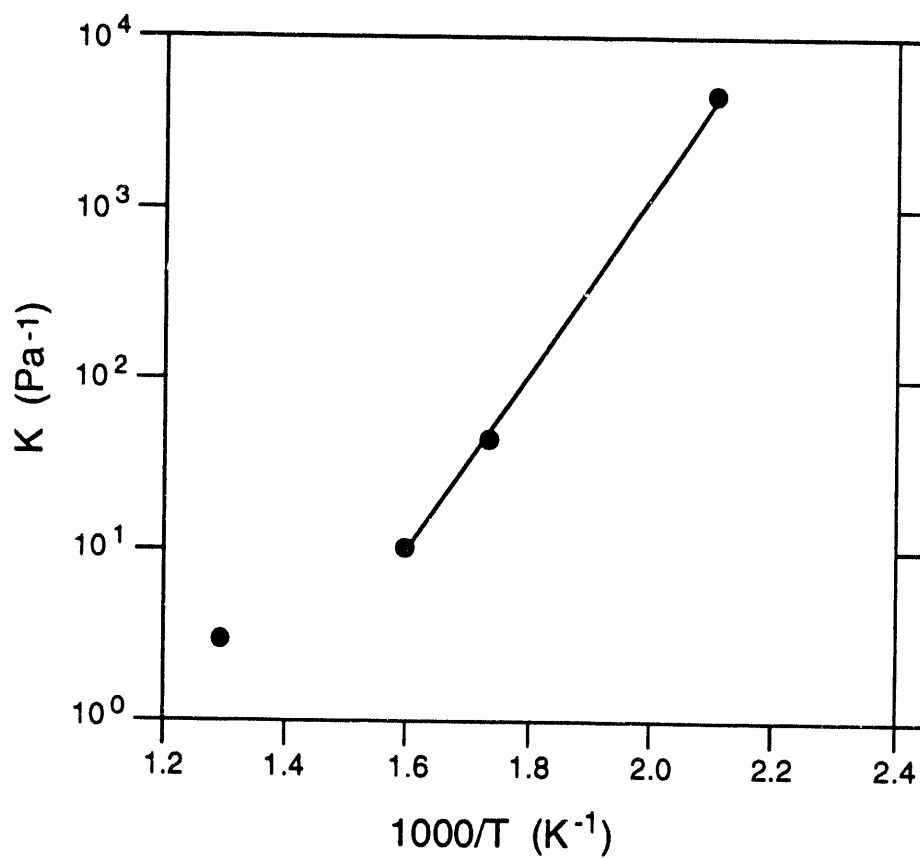


Figure 11. van't Hoff Plot of the Equilibrium Constants

X-Ray Diffraction Analysis of Deuterium-Loaded Samples

We analyzed samples of St 198 from absorption isotherm measurements by XRD to see if changes that occurred during reaction with deuterium could be detected. Activation of St 198 caused no changes in the XRD pattern. Table 5 shows relative intensities of the strongest XRD peaks for several phases in deuterium-loaded samples as a function of temperature. Figure 12 shows diffraction patterns for the samples in Table 5. While XRD peaks for Zr_2Fe , $ZrFe_2$, α -Zr, and Zr_6Fe_3O are dominant phases as-received material, the addition of deuterium for 200°C causes the Zr_2Fe , α -Zr, and Zr_6Fe_3O peaks to disappear. Disappearance of the Zr_2Fe peak is explained by the formation of Zr_2FeD_x , as indicated by the Zr_2FeD_x peaks at 200°C. Alpha-zirconium probably forms $ZrD_{1.8}$ but the absence of $ZrD_{1.8}$ peaks is surprising, and may form amorphous $ZrD_{1.8}$ or very small $ZrD_{1.8}$ domains. Zr_6Fe_3O , which was detected in the as-received material, was no longer present in samples exposed to formation 350°C or less. This result suggests that Zr_6Fe_3O may be reduced to Zr_2Fe during absorption of deuterium at 200°C to 350°C.

Table 5. Relative Intensities of the Strongest XRD Peaks for As-Received and Deuterium-Exposed SAES St 198

| Phase | Zr_2Fe | $ZrFe_2$ | α -Zr | Zr_6Fe_3O | Zr_2FeD_x | $ZrD_{1.8}$ |
|-------------|----------|----------|--------------|-------------|-------------|-------------|
| As-Received | 100 | 76 | 49 | 53 | 0 | 0 |
| 200 | 0 | 23 | 0 | 0 | 100 | 0 |
| 300 | 0 | 24 | 0 | 0 | 100 | 24 |
| 350 | 0 | 34 | 0 | 0 | 100 | 21 |
| 400 | 0 | 55 | 0 | 38 | 29 | 100 |
| 500 | 0 | 57 | 0 | 35 | 0 | 100 |

$ZrD_{1.8}$ peaks are absent in the as-received and 200°C samples, but become apparent in samples exposed at 300°C and 350°C. These become the most intense peaks in the diffraction patterns at 400°C and 500°C. The Zr_2FeD_x peak becomes less intense at 400°C, and is absent at 500°C. Thus, on the time scale of our experiments, Zr_2FeD_x is stable at temperatures of 350°C and below. Above 350°C, Zr_2FeD_x decomposes rapidly. The reason for the reappearance of Zr_6Fe_3O peaks at 400°C and 500°C is unclear. Observation of the diffraction patterns, as well as the data in Table 5, indicate an intensity increase in the $ZrFe_2$ peaks. It appears that there may be an increase in the $ZrFe_2$ peak intensity at higher temperatures.

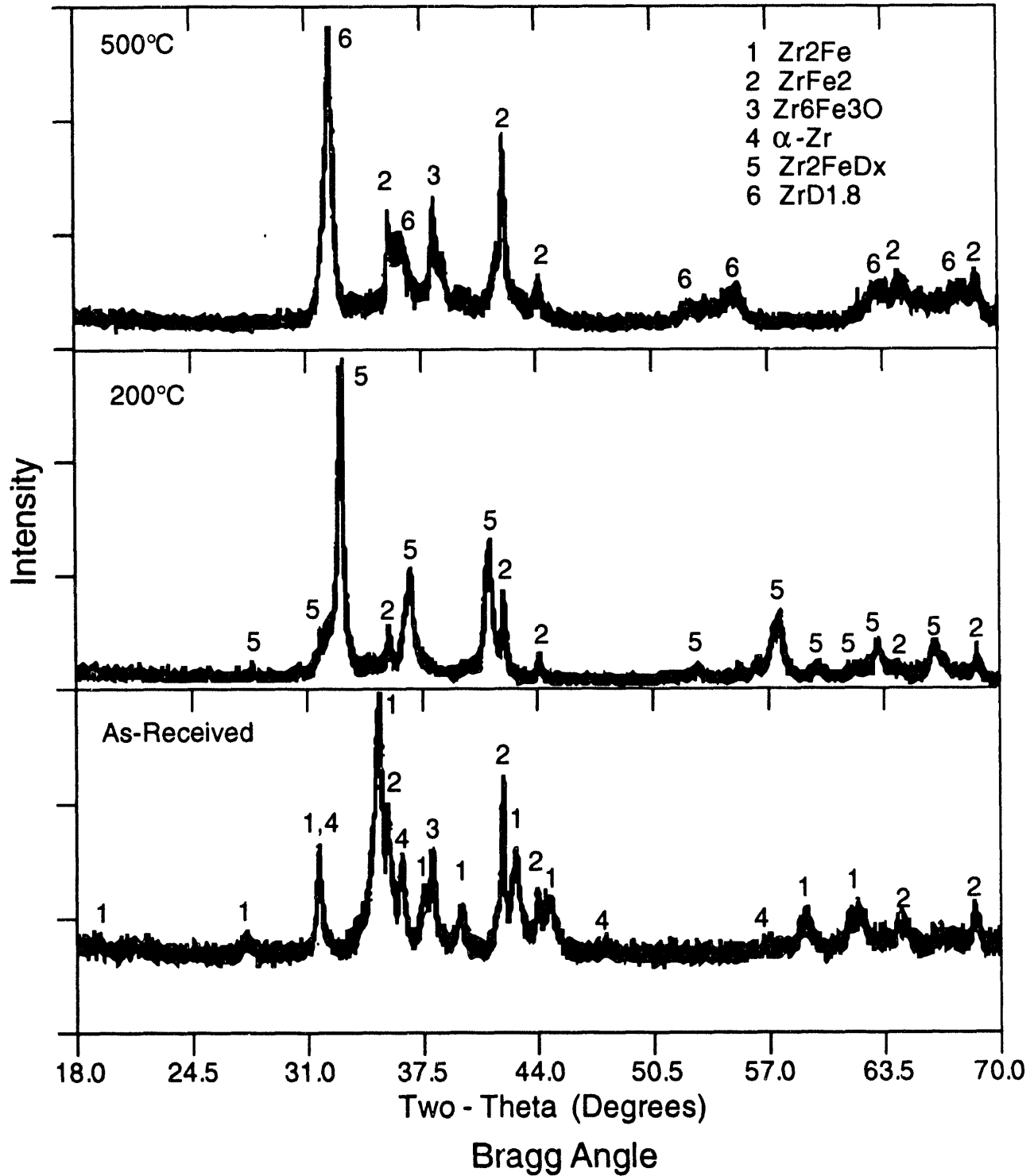


Figure 12. X-Ray Powder Diffraction Patterns of SAES St 198 Samples After Conducting Absorption Isotherms at 200°C and 500°C

Discussion

Elemental analyses of St 198 detected tin in addition to zirconium and iron. It is uncertain if tin is an impurity or is an intentional addition. All other elements are present at impurity levels, and probably do not significantly influence the deuterium absorption behavior of St 198. Detection of primary Zr_2Fe by SEM and XRD is consistent with the elemental analysis and the Zr-Fe binary phase diagram.⁸ The Zr-Fe phase diagram indicates that elemental zirconium should be the secondary phase in eutectic. However, Zr_3FeSn is present along with only pure zirconium (as α -Zr) as a secondary phase in eutectic. Thus, tin appears to play a role in the eutectic behavior of Zr_2Fe . Because no Zr_3FeSn XRD peaks were detected, it is possible that this phase is amorphous. The cubic phase identified as Zr_6Fe_3O seemingly results from oxygen contamination of Zr_2Fe . The iron-zirconium phase diagram indicates that, at temperatures less than 775°C, Zr_2Fe is unstable and will undergo a transformation to Zr_3Fe and $ZrFe_2$. Evidently, the kinetics of this transformation is slow because no Zr_3Fe was detected in any of our samples. The absence of Zr_3Fe in our samples is surprising because it is often detected in cast and annealed binary zirconium-iron alloys with compositions similar to St 198.⁹

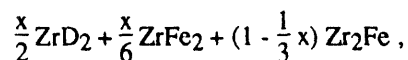
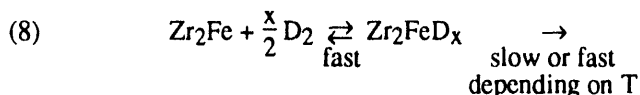
Results from the activation study indicate that, at the lower activation temperature (350°C) and under poor vacuum conditions, initial deuterium absorption rates were significantly lower. At the higher activation temperature (500°C), deuterium absorption rate is not influenced by vacuum conditions, and is rapid for both poor and good vacuum quality. Most likely, the higher gas-phase oxygen, water, and other impurity concentrations under poor vacuum conditions cannot be adsorbed and diffused into the bulk at a sufficiently fast rate to maintain a clean and active getter surface. At the higher temperature, adsorption and diffusion of impurities into the bulk is rapid. There is little buildup of these impurities on the surface. The main effect value for the influence of activation time on the activation process (Table 4) indicates that time has a small effect on the activation of St 198.

While measuring absorption isotherms at 400°C and 500°C, we noticed that a slow reaction, which consumed deuterium, may be occurring in the lattice (Figure 9). The XRD results presented in Table 5 and in Figure 12 indicate that on the time scale over which our samples were exposed, Zr_2FeD_x begins to decompose rapidly above 350°C. While it is clear that this decomposition proceeds with formation of $ZrD_{1.8}$, the state of the remaining iron is not certain. Previous investigators indicate that Zr_2FeH_x proceeds with formation of ZrH_2 and $ZrFe_2$. Van Essen and Buschow⁵ indicate that for 4 hours at 50°C and under hydrogen pressure of 4.05 MPa, the reaction of hydrogen with Zr_2Fe forms ZrH_2 and $ZrFe_2$. Although these authors indicate that results from x-ray diffraction led to this conclusion, the details of their x-ray diffraction results were not provided. It is uncertain from the Van Essen and Buschow paper which of the decomposition products (ZrH_2 or $ZrFe_2$) they detected. It is surprising that the decomposition products were detected at such a low temperature. However, the extremely high hydrogen pressure used may cause this. From XRD analysis of samples, Aubertin et al.⁶ also report the formation of ZrH_2 and $ZrFe_2$. Their samples were exposed to temperatures of 850°C, where migration of atoms is sufficiently fast to allow to form significant quantities of additional phases such as ZrH_2 and $ZrFe_2$. Manini et al.³ examined the phases present in Zr_2Fe samples fully and partially loaded with hydrogen. XRD analysis of their partially loaded

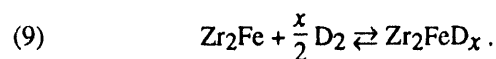
samples suggests some formation of $ZrFe_2$, whereas $ZrFe_2$ peaks in diffraction patterns of the fully loaded samples were distinct. Their samples were held at 500°C for 2 hours.

The XRD results in Table 5 and in Figure 12 indicate that, while it is clear that $ZrD_{1.8}$ is forming at the higher temperatures, formation of $ZrFe_2$ at the higher temperatures (> 350°C) is not obvious. Our samples were exposed to deuterium for ~ 8 hours, which is significantly longer than the samples that Manini et al. examined. The deuterium loading of our samples was not constant, so a straightforward comparison between our samples and the Manini et al. samples is not possible. However, the 500°C absorption isotherms in Figure 9 that were collected for equilibration times of 20 minutes and 1 hour indicate that at low loading (<2 kPa.L.g) there is little difference between the two isotherms. As loading increases, the decomposition reaction is more rapid. Apparently, the decomposition reaction rate increases with loading. Thus, it is likely that fully loaded Zr_2Fe samples that Manini et al.³ and Aubertin et al.⁶ examined had significantly higher decomposition rates because they were fully loaded.

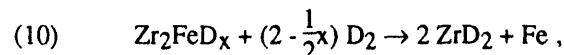
Our samples are probably similar to the partially loaded samples of Manini et al. that showed minor formation of $ZrFe_2$. The reaction of deuterium with Zr_2Fe and subsequent decomposition of Zr_2FeD_x to ZrD_2 and $ZrFe_2$ can be described as follows:



where $0 < x < 3$. The first step is a rapid equilibration. The second step is slow at low temperatures, and becomes faster at higher temperature. Zr_2Fe formed in Equation (8) subsequently reacts with deuterium from the gas phase to restore the equilibrium concentration of Zr_2FeD_x .



This explains the observed slow deuterium consumption from the gas phase. Equation (8) predicts stoichiometric formation of $ZrFe_2$. However, Table 5 indicates that while formation of ZrD_2 is distinct, there is only a slight indication of $ZrFe_2$ formation. Therefore, Equation (8) cannot fully explain the behavior. It is also possible that Zr_2FeD_x could decompose to ZrD_2 without forming $ZrFe_2$. For example,



could proceed with formation of Fe as well as ZrD_2 . Our XRD results do not detect metallic iron, although iron produced in this reaction might not crystallize to sufficiently large crystals to be detected by XRD. Similar high-temperature disproportionation reactions have been observed with other

intermetallic compounds, where the element having high hydrogen affinity reacts to form a stable metal hydride. It is likely that both Equations (8) and (10) are occurring.

The inherent instability of the Zr_2Fe compound, as dictated by the Zr-Fe phase diagram⁸, indicates that at temperatures less than 775°C Zr_2Fe should transform to Zr_3Fe and $ZrFe_2$ in the absence of hydrogen isotopes. In the presence of hydrogen isotopes, decomposition occurs by Equations (8) and (10). We detected little decomposition of Zr_2Fe in deuterium-loaded samples at 350°C after about 8 hours. However, in recent experiments with St 198 (to be reported in the future) where the material was held at 350°C while loaded with deuterium for longer periods of time (>5 days), we see significant decomposition of Zr_2Fe , as indicated by strong $ZrD_{1.8}$ XRD peaks. Thus, decomposition of Zr_2Fe can be expected in applications involving high temperature and significant hydrogen isotope loading. For applications such as tritium removal from glovebox atmospheres or process gas streams, extended exposure of the material to high temperature (350°C) will be the case, but very low tritium loadings are expected. Figure 9 indicates that decomposition of Zr_2Fe at a loadings less than about 2 kPa·L·g⁻¹ is slow even at 500°C.

Although previous investigators have indicated that tritium recovery and regeneration of St 198 capacity can be achieved by heating the alloy to 700°C under vacuum or under noble gas purge,² we believe that an investigation is needed to fully characterize this process. Heating tritium-loaded St 198 to high temperature will likely cause the reaction of some tritium to form ZrT_2 . While some tritium will be recovered, it is likely that a portion of the tritium will be converted irreversibly to ZrT_2 . Furthermore, the regenerated material would show a decreased capacity for getting tritium, and possibly other material differences from the freshly activated St 198. A further investigation is probably necessary to establish the optimum regeneration conditions.

It was shown above that the P-C-T data can be correlated with a simple equilibrium expression (Equation [7]). While previous investigators have used a different expression to correlate P-C-T data for Zr_2Fe ,^{3,4} Equation (7) represents an improvement to the previous expressions because it applies to the full range of deuterium loadings. Because of secondary reactions occurring in the lattice at temperatures above 350°C, it is not possible to provide a reliable correlation at temperatures above 350°C.

Analysis of the P-C-T data resulted in an absorption enthalpy (ΔH_a) of 101.8 kJ·mole⁻¹ D₂. Other investigators have measured ΔH_a values for other SAES getters. ΔH_a for deuterium absorption in St 101 is reported to be 138.2 kJ·mole⁻¹ D₂; ^{10, 11} ΔH_a for St 707 is 120.6 kJ·mole⁻¹ D₂.¹⁰ St 101 has much lower absorption pressures than St 198, and it thus should have a higher absorption enthalpy. The absorption pressures of St 198 are similar to those of St 707, so a similar absorption enthalpy is expected, but the value for St 198 that we report is lower than that of Boffito et al.¹⁰ However, the absorption enthalpy reported by Boffito et al. was determined from P-C-T data for low deuterium loading in the alloy. Our absorption enthalpy result for St 198 was extracted from P-C-T data covering the full deuterium capacity of the alloy. Because of repulsive interaction effects between deuterons in the metal lattice, the absorption enthalpy is most likely a function of the alloy deuterium loading. Repulsive interactions would likely cause lower absorption enthalpy at higher deuterium loading, and this may be the reason for our lower absorption enthalpy value.

Conclusion

St 198 consists mostly of the Zr_2Fe phase with secondary phases of $ZrFe_2$, Zr_5FeSn , $\alpha-Zr$, and Zr_6Fe_3O . The material becomes well activated when evacuated at temperatures higher than $350^\circ C$ for 4 hours or longer, as long as a relatively high vacuum is maintained. Higher activation temperatures should be considered for systems with poorer vacuum quality. Deuterium P-C-T data for the full range of getter deuterium loadings and at temperatures of $350^\circ C$ or lower can be correlated using a simple equilibrium expression. At temperatures higher than $350^\circ C$, Zr_2FeD_x decomposes at a significant rate to ZrD_2 , and possibly $ZrFe_2$ and Fe. However, for applications involving low hydrogen isotope loading, such as stripping low tritium concentrations from glovebox or process atmospheres, the decomposition reaction probably would be insignificant. Recovery of tritium absorbed on St 198 by heating under vacuum at temperatures higher than $500^\circ C$ would likely cause decomposition of Zr_2FeT_x with the formation of irreversible ZrT_2 , and a decreased capacity of the regenerated material. An investigation is necessary to establish the feasibility and optimum conditions for recovering hydrogen isotopes from St 198.

Acknowledgments

The authors wish to thank many individuals for contributions to this work. Mercury porosimetry was performed by R. A. Malstrom, bulk elemental analyses by plasma-mass spectroscopy and x-ray fluorescence were provided by C. J. Coleman and A. R. Jurgensen, respectively. F. E. Odum and A. S. Holston prepared the samples for scanning electron microscopy and electron probe microanalysis. Scanning electron microscopy examination was performed by A. S. Holston and J. E. Durden. Electron probe microanalysis was performed by L. F. Tovo and S. F. McDaniel. A. R. Jurgensen and R. E. Howell provided the x-ray diffractometry analyses. W. L. Moyer assisted with the activation study and P-C-T measurements.

References

1. Kherani, N. P., Shmayda, W. T., and Jalbert, R. A., *Proceedings of the 12th Symposium on Fusion Engineering*, Monterey, Ca., October 12-16, 1987, I. E. Conf. No. 11702.
2. Shmayda, W. T., Kherani, N. P., Wallace, B., and Mazza, F., *Fusion Technology*, Vol. 21, 616 (1992).
3. Manini, P., Boffito, C., Gasparini, G., Maran, C., and Gallitognotta, A., *Proceedings of the 2nd European Vacuum Conference*, Trieste (1990).
4. Boffito, C., Doni, F., and Rosai, L., *Journal of the Less-Common Metals* 104, 149 (1984).
5. Van Essen, R. M., and Buschow, K. H. J., *Journal of the Less-Common Metals* 64, 277 (1979).
6. Aubertin, F., Gonser, U., and Campbell, S. J., *Journal of the Less-Common Metals* 101, 437 (1984).
7. Powder Diffraction Files compiled by the JCPDS - International Center for Diffraction Data.
8. Massalski, T. B., Editor-in-Chief, "Binary Alloy Phase Diagrams", Second Edition, Volume 3, p. 1798, ASM International (1990).

9. Malakhova, T. O., and Alekseyeva, Z. M., *Journal of the Less-Common Metals* 81 293 (1981).
10. Boffito, C., Ferrario, B., and Martelli, D., *Journal of Vacuum Science and Technology A* 1 (2), 1279 (1983).
11. Knize, R. J., *Journal of Vacuum Science and Technology* 20, 1135 (1982).

This page intentionally left blank.

DISTRIBUTION

Copy No.

1. J. R. Knight, 773-A
2. T. Motyka, 773-A
3. J. R. Dollar, 232-H
4. A. F. Reichman, 773-A
5. M. W. Lee, 773-A
6. A. Nobile, LANL, MST-3, C 348
7. W. C. Mosley, 773-A
8. J. S. Holder, 232-H
9. K. N. Brooks, 234-H
10. J. R. Wermer, 232-H
11. J. E. Klein, 773-A
12. L. K. Heung, 773-A
13. D. L. Hayes, 235-H
14. D. J. Green, 235-H
15. R. A. Pedde, 235-H
16. R. D. Buley, 233-5H
17. W. B. Wilson, 703-42A
18. B. S. Strack, 703-43A
19. C. W. Tope, 703-43A
- 20-23. TIM, 703-43A

END

**DATE
FILMED**

4 / 11 / 94

